

# Event-based Camera Tracker by $\nabla_t$ NeRF

Mana Masuda\*, Yusuke Sekikawa†, Hideo Saito\*

\*Keio University, †Denso IT Laboratory

{mana.smile, hs}@keio.jp, ysekikawa@mail.d-itlab.co.jp

## Abstract

*When a camera travels across a 3D world, only a fraction of pixel value changes; an event-based camera observes the change as sparse events. How can we utilize sparse events for efficient recovery of the camera pose? We show that we can recover the camera pose by minimizing the error between sparse events and the temporal gradient of the scene represented as a neural radiance field (NeRF). To enable the computation of the temporal gradient of the scene, we augment NeRF’s camera pose as a time function. When the input pose to the NeRF coincides with the actual pose, the output of the temporal gradient of NeRF equals the observed intensity changes on the event’s points. Using this principle, we propose an event-based camera pose tracking framework called TeGRA which realizes the pose update by using the sparse event’s observation. To the best of our knowledge, this is the first camera pose estimation algorithm using the scene’s implicit representation and the sparse intensity change from events.*

## 1. Introduction

Camera localization/tracking is one of the fundamental functionality of computer vision. The field of use lies in many applications like automotive, augmented reality, and robotics. Event-based cameras detect sparse intensity changes with extremely high temporal resolution ( $>10,000$  fps). This unique feature makes it a suitable sensor for tracking fast-moving scenes, and many researchers have been exploring several approaches to utilize high-speed observation. Recently, [10, 21] showed the pose & motion is recovered by minimizing the error between the estimated intensity change and integrated events (Fig.2). Thanks to the low-latency nature of events, their method works well even in a rapid camera motion. However, they need a dense operation to differentiate the error w.r.t pose & motion; it could not take advantage of the *sparsity* of events. Therefore, the computational cost increases linearly with the processing rate, making it difficult to run the algorithm in real-time on devices with limited computational resources.

NeRF [37] is an implicit light-field representation using a neural network, which enables unified perceptions of the 3D world that is difficult for the existing explicit MAP (e.g., CAD model). Many NeRF-extention have been proposed [54] to model a complex 3D scene; we believe these advancements make the NeRF representation a novel candidate for representing 3D MAP for camera localization/tracking. Utilization of NeRF as a 3D MAP for camera pose localization has already been explored [30, 62]. Their basic idea for realizing camera pose estimation is minimizing the error between the estimated intensity frame from NeRF and the observed intensity frame, w.r.t input camera pose (Fig.3). However, these methods can not estimate the camera pose by using sparse intensity change.

These existing studies motivate one question; how can we utilize sparse events to recover the camera pose without converting them into dense frames? We show:

Pose is recovered by minimizing  $|\nabla_t \text{NeRF}(S_t) - \text{event}|$ .

When coordinates of events (where the event camera detects intensity changes) and the current camera pose estimate on the event’s time  $S_t$  are input to NeRF, it outputs the intensities at that point and time. By viewing the input camera pose to NeRF as a function of time, we found that the temporal gradient of the intensity w.r.t the event’s timestamp is the estimation of intensity changes on that pixel. Pose & motion is obtained by minimizing  $|\text{estimated intensity changes} - \text{observed intensity changes (events)}|$  (Theorem-1, Fig.1).

Based on this principle, we propose an event-based camera pose tracking framework called minimization of the  $\nabla_t \text{NeRF}(S_t)$  (TeGRA). Unlike the conventional dense approach (frame-based), which operates in intensity-space, TeGRA works sparsely (event-based) in gradient-space; it updates the pose & motion by evaluating the error only for the pixels where the events have been observed. By the sparse mechanism, the number of pixels to be evaluated is **99.8% less** than the conventional dense algorithm on our created event dataset. To the best of our knowledge, this is the first approach to realizing camera pose estimation using the implicit representation of the 3D scene and the sparse observation of intensity changes. We provide

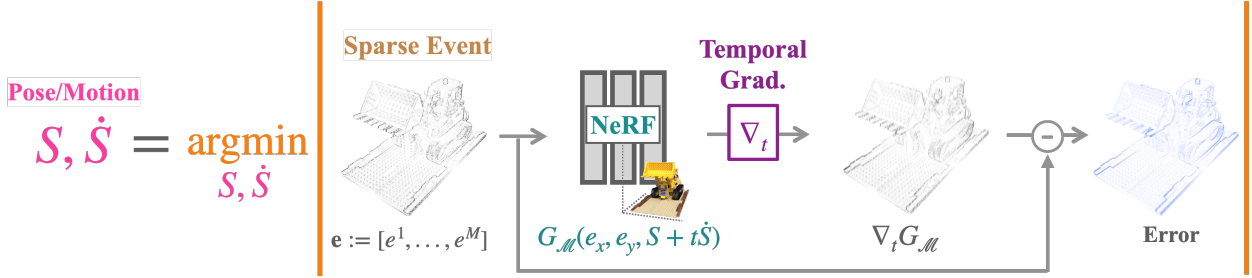


Figure 1.  $\text{argmin} |\text{Temp. Grad. of } \text{NeRF}(S_t) - \text{Event}|$  is Pose & Motion.

the theoretical proof of TeGRA. Furthermore, we created a photo-realistic event dataset for 6DoF camera pose tracking with a ground-truth pose called EvTrack (EVent-based TRACKing dataset). Using the EvTrack, we experimentally proved the concept.

## 2. Related Work

### 2.1. Camera Pose Tracking from Intensity Frame

There is a long history in the field of camera pose tracking. Many algorithms are based on frame-based observation, namely video sequence. Methods based on KLT [5, 34] are among the most popular visual tracking algorithms. KLT computes the camera pose by aligning the observed intensity frame with the known scene's intensity map using an image gradient. Recently, the deep neural network (DNN) based feature extractor has been utilized to exploit more rich features [13] than the raw pixel value. This KLT-based method works well in many scenarios. However, it easily collapses in a fast-moving scene, which induces a significant difference between the observed frame and the estimated frame. The difference makes the gradient-based algorithms trapped into a local minimum. Another line of research utilizes DNN to directly regress the pose between pairs of images [7, 8, 26, 28, 55]. They have an advantage in computational efficiency (over the iterative gradient-based algorithm) because they can update the pose by a single forward pass of the network. They may also suffer from performance degeneration when there is a significant difference in the pairs of images due to the fast camera motion.

Either gradient-based or regression-based, the problem due to the fast camera motion might be mitigated by using an expensive high-speed camera. However, processing them at a higher rate is infeasible due to increased computational complexity.

### 2.2. Camera Pose Tracking from Events

An event-based camera [14, 43, 44, 49, 53] is a bio-inspired vision sensor that mimics biological retinas. It differs from a frame-based camera in its H/W design; its report per-pixel intensity changes as asynchronous event

streams. Thanks to this unique operation principle, event-based cameras have significant advantages over conventional frame-based cameras, e.g., low latency, high dynamic range (HDR), and blur-free. The most important feature of the event-based camera for camera pose tracking would be its high temporal resolution. Their temporal resolution is equivalent to  $>10,000$  fps, making it a suitable sensor for robust tracking in fast-moving scenes.

**Use of Event frame for Camera Pose Estimation.** There have been many attempts to utilize the distinct features of the event-based camera for tracking [1, 2, 10, 12, 19, 21, 22, 47, 67]. Recently, KLT has been extended to event data to realize robust camera pose tracking in high-speed and HDR scenarios [10, 21, 22]. They update camera pose and motion by minimizing the error in the integrated event frame between estimation and observation (Fig. 2). The estimation is computed from the current estimate of the pose & motion using the pre-build 3D intensity map. By utilizing the low-latency nature of events, their methods work well even in rapid camera motion. However, computing the derivatives of the error w.r.t pose requires computationally intensive dense rendering of the 3D map. The dense computation needs to be repeated until convergence for each frame. Therefore, running the algorithm in real-time on devices with limited computational resources is difficult. Our goal in this study is to realize an efficient sparse algorithm for camera pose tracking using the implicit representation of a 3D scene.

### 2.3. Implicit Scene Representations

Representing data, such as image, video, and shape using implicit neural representation gained much attention such as for data compression [15, 35], novel-view synthesis [36–38], 3D-shape modeling [3, 11, 40, 50], and image registration [30, 62] to name a few. NeRF [37] utilizes the implicit neural representations to represent the 4D light-field. Given a set of images paired with a camera pose, NeRF learns the intensities of each pixel for a given camera pose. Each pixel's intensity is computed by integrating the RGB color and density along the corresponding ray using the volumetric rendering technique. Due to its flex-

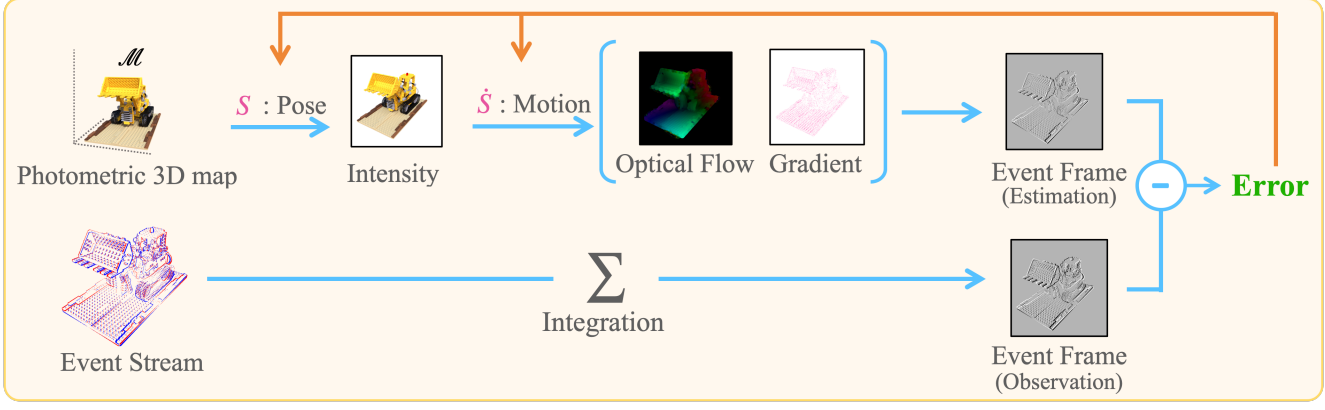


Figure 2. Tracking using event stream and explicit scene

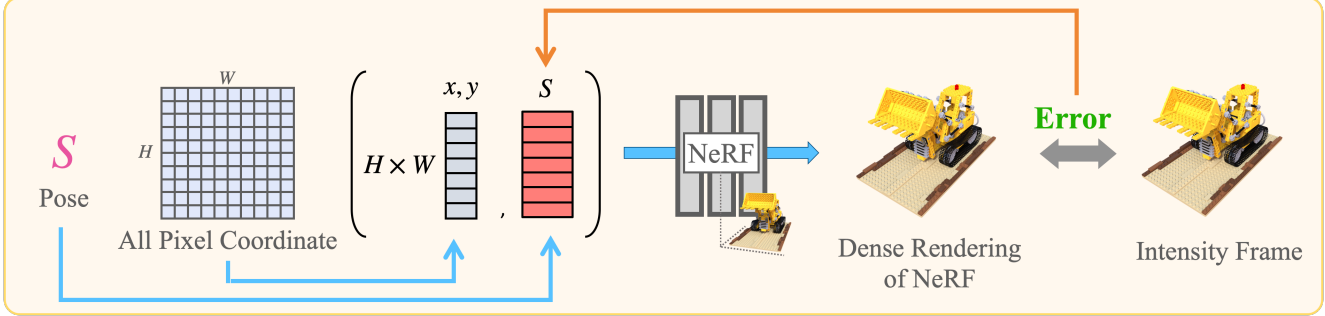


Figure 3. Tracking using intensity frame and implicit scene

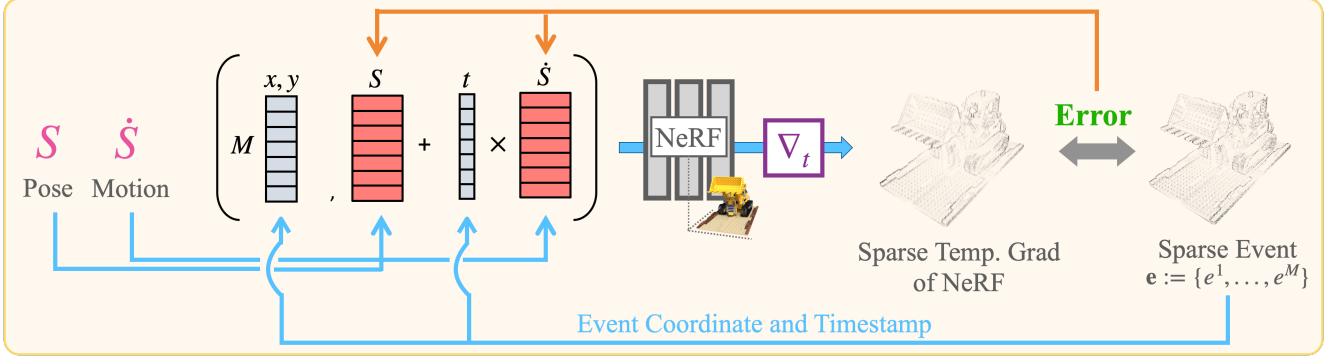


Figure 4. Tracking using event stream and implicit scene (TeGRA)

ibility, NeRF extensions are exploding beyond its original application of novel-view synthesis; e.g., 3D-shape reconstruction [39, 56], disentangle lighting [9, 51, 59, 64], image editing [25, 33, 61], object separation [4, 60], semantic label propagation [65], modeling time-varying objects [18, 27, 29, 32, 41, 45], and depth estimation [24, 58].

**Use of NeRF for Camera Pose Estimation** These novel functionalities realized by NeRF such as modeling lighting and moving objects would realize a unifying perception of the 3D world that is difficult for the existing explicit MAP

(e.g., CAD model). Furthermore, recent progress of NeRF-extention enabled it to model a large environment, such as a large house [17], and an entire city [54]. We believe these advancements make the NeRF representation a novel candidate for representing 3D MAP for camera localization/tracking. iNeRF [62] uses the inverse of NeRF to estimate the camera pose. BARF [30], NeRF- [57], iMAP [52], NICE-SLAM [66] realized simultaneous camera pose estimation and 3D scene reconstruction. Their basic idea for realizing camera pose estimation is minimizing the error

between the estimated intensity frame from NeRF and the observed intensity frame, w.r.t input camera pose (Fig.3). These methods can not estimate the camera pose by using sparse intensity change. We aim to derive a camera pose tracking algorithm using sparse intensity changes observation (i.e., events) to realize efficient camera pose tracking.

### 3. Method

#### 3.1. Preliminaries

**Problem Statement** Our goal in this study is to develop an efficient camera pose tracking algorithm TeGRA using sparse observation of intensity-change event (IC-event) stream  $\mathbf{e}_t$  as follows:

$$\text{TeGRA} : (\mathbf{e}_t, S_t^{\text{ini}}, \dot{S}_t^{\text{ini}}) \mapsto (S_t^{\text{opt}}, \dot{S}_t^{\text{opt}}), \quad (1)$$

where  $(S_t^{\text{ini}}, \dot{S}_t^{\text{ini}})$  and  $(S_t^{\text{opt}}, \dot{S}_t^{\text{opt}})$  are the initial and optimized pose & motion at time  $t$  respectively. TeGRA utilizes a differentiable implicit representation of the static 3D world.

**NeRF** This study assumes that the 3D scene is implicitly represented by NeRF [37]. NeRF,  $G_{\mathcal{M}}$  was initially proposed for novel-view synthesis; it represents the scene using a neural network that is differentiable w.r.t to its input pose  $S$ . The parameter of the NeRF,  $\mathcal{M}$ , is pre-trained before tracking. NeRF  $G_{\mathcal{M}}$  takes an image coordinate  $(x, y)$  and 6DoF pose  $S \in \text{se}(3)$  of the camera as inputs and renders the RGB intensity  $\mathbf{c}$  at that coordinate;

$$G_{\mathcal{M}}(x, y, S) = \mathbf{c}. \quad (2)$$

**IC-Event** The IC-event stream  $\mathbf{e}_t$  is a set of events observed in time interval  $[t, t + \tau]$  as follows:

$$\mathbf{e}_t = [e^1, \dots, e^i, \dots, e^M]; \quad e^i = [e_x^i, e_y^i, e_u^i, e_r^i]^T, \quad (3)$$

where  $(e_x^i, e_y^i) \in \mathbb{R}^2$  is the image coordinates where the intensity change has been detected,  $e_u^i \in \mathbb{R}$  is the timestamp of the change, and  $e_r^i \in \mathbb{R}$  is the intensity change value. The intensity change value  $e_r(x, y)$  on  $(x, y)$  within time interval  $\Delta t$  is defined using *true* intensity  $L(x, y, t)$  as follows:

$$e_r(x, y) = \frac{L(x, y, t + \Delta t) - L(x, y, t)}{\Delta t}. \quad (4)$$

Events are detected where the intensity change  $e_r(x, y)$  exceeds the predefined threshold  $\delta$ . For ease of discussion, we define  $\bar{e}_u^i$ , which is relative timestamp w.r.t time  $t$ ;  $\bar{e}_u^i := e_u^i - t$ . That is  $\bar{e}_u^i$  changes depending on the time  $t$  we consider. Some event-based cameras directly detect the intensity change  $e_r$ , such as Celex-V [14], or IC-event is obtained from high-speed video data. We left the evaluation using the binary event for future work<sup>1</sup>.

<sup>1</sup>At this time, we consider there are two possible approaches to make

#### 3.2. The answer of $\nabla_t \text{NeRF}(S_t) = \mathbf{0}$ is true pose & motion

By viewing the input camera pose to NeRF as a function of time, we found that camera pose & motion  $(S, \dot{S})$  can be recovered by minimizing the error between the temporal gradient of the 3D-scene represented as NeRF  $G_{\mathcal{M}}$  and IC-event stream  $\mathbf{e}$  (Fig.5: visual explanation).

**Theorem 1.** *The minimizer of  $|\nabla_t \text{NeRF}(S_t) - \text{event}|$  is true pose & motion  $(S_t^{\text{gt}}, \dot{S}_t^{\text{gt}})$ :*

$$S_t^{\text{gt}}, \dot{S}_t^{\text{gt}} = \underset{S, \dot{S}}{\operatorname{argmin}} \sum_i \underbrace{\left\| \frac{\partial G_{\mathcal{M}}(e_x^i, e_y^i, S_t + \bar{e}_u^i \dot{S}_t)}{\partial e_u^i} - e_r^i \right\|_2}_{:= \mathcal{L}}. \quad (5)$$

*Proof.* To prove the theorem-1, we'll show the  $i$ -th element of the Eq.(5) equals to zero when we have the true pose & motion  $(S_t^{\text{gt}}, \dot{S}_t^{\text{gt}})$ . Now, consider the temporal gradient of the NeRF of Eq.(2) for  $i$ -th event on time  $e_u^i$ :

$$\begin{aligned} & \frac{\partial G(e_x^i, e_y^i, S_t + \bar{e}_u^i \dot{S}_t)}{\partial \bar{e}_u^i} \\ &= \lim_{\Delta u \rightarrow 0} \frac{G(e_x^i, e_y^i, S_t + (\bar{e}_u^i + \Delta u) \dot{S}_t) - G(e_x^i, e_y^i, S_t + \bar{e}_u^i \dot{S}_t)}{\Delta u} \end{aligned} \quad (6)$$

From the definition of NeRF of Eq.(2),  $L(x, y, t)$  equals to the NeRF's output, when the estimated pose & motion is true:

$$L(x, y, t + \bar{e}_u^i) = G(x, y, S_t^{\text{gt}} + \bar{e}_u^i \dot{S}_t^{\text{gt}}). \quad (7)$$

Plugging this relation to Eq.(6)

$$\begin{aligned} & \frac{\partial G(e_x^i, e_y^i, S_t^{\text{gt}} + \bar{e}_u^i \dot{S}_t^{\text{gt}})}{\partial \bar{e}_u^i} \\ &= \lim_{\Delta u \rightarrow 0} \frac{L(e_x^i, e_y^i, t + \bar{e}_u^i + \Delta u) - L(e_x^i, e_y^i, t + \bar{e}_u^i)}{\Delta u} \\ &= \lim_{\Delta u \rightarrow 0} \frac{L(e_x^i, e_y^i, e_u^i + \Delta u) - L(e_x^i, e_y^i, e_u^i)}{\Delta u} \end{aligned} \quad (8)$$

This equals to the definition of  $e_r^i$  of Eq.(4) when  $\Delta t$  is sufficiently small.  $\square$

TeGRA compatible with the binary-event; 1) Modify the loss function of (5) to adapt to the binary-event (Sec.5.2), 2) Convert the binary-event to IC-event using the timestamp (supplement-D). In this work, we use IC-event for simplicity and left the exploration for future work.

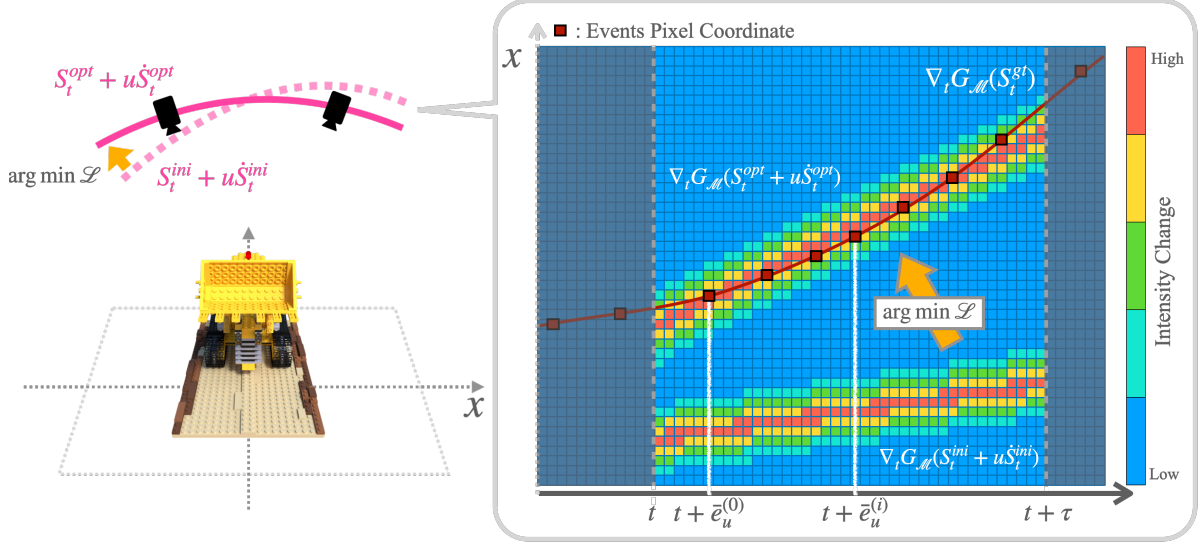


Figure 5. Pose & motion estimation (visual explanation of theorem-1)

### 3.3. Sparse Tracking Algorithm: TeGRA

Using the theorem-1, we propose an event-based camera pose-tracking algorithm called TeGRA. The algorithm minimizes  $\mathcal{L}$  in Eq.(5) using gradient-decent (Fig. 4). The input to TeGRA is the IC-event stream  $e_t$  at time  $t$  and the initial estimate of pose & motion  $(S_t^{\text{ini}}, \dot{S}_t^{\text{ini}})$ . To obtain the derivative to update pose & motion, we differentiate the loss  $\mathcal{L}$  w.r.t  $(S_t, \dot{S}_t)$  through the temporal gradient of  $G_M$  on each event's timestamp  $e_u^i$ . Then, pose & motion is updated using the sum of all events contributions. See listing 1 for pseudo-PyTorch code.

## 4. Experiments

To demonstrate the effectiveness of the proposed TeGRA, we created the 6DOF camera pose tracking dataset for event data, called EvTrack, with ground-truth camera pose. We used BOP challenge 2020 scenes [23] because it is photo-realistic, and the scene well represents the indoor localization scenario. The BOP uses the BlenderProc [16] to render realistic images using ray tracing. We first show the tracking result of TeGRA for proof of concept (POC) (Sec.4.3). Next, we show the intensive qualitative comparison with a dense algorithm (Fig.3) using intensity in terms of pose estimation accuracy (Sec.4.4).

### 4.1. Event-based camera pose tracking dataset (EvTrack)

The dataset consists of five scenes, *mix*, *hb*, *lm*, *tyol* and *ycbb*, the last four scenes correspond to the BOP data split and *mix* scenes include all the four data to simulate the ordinary indoor situation. We used *mix* scene for proof of concept in the tracking scenario and use the other four for

the quantitative evaluation in terms of pose estimation accuracy. We generated 500 images for NeRF training and three camera trajectories (Fig.6 right) for each of the five scenes simulating the drone hovering around a room. The IC-event stream is generated by using pairs of consecutive images (total of 1,000),  $\{L(t), L(t+\nu)\}$  ( $L(t) \in \mathbb{R}^{H \times W}$ ), by subtracting them. The size of image ( $H, W$ ) is  $(480 \times 640)$ . The threshold  $\delta$  for triggering the event is set to 0.05 (intensities are normalized to  $[0, 1]$ ) for all scenes. In our experiment, we converted the RGB IC event to a grayscale IC event since most event cameras detect grayscale intensity changes. Each event stream is generated using five consecutive frames, assuming the motion is approximately linear within the interval.

### 4.2. Implementation

We use Pytorch [42] to train the NeRF-model and run TeGRA for tracking<sup>2</sup>.

**Training** We follow the network settings from the original NeRF with minor modifications; use the softplus activation for the volume density  $\sigma$  as recommended in BARF [30] for improved stability.

**Tracking** We add the RGB-to-gray layer (Sec.3.3) to use grayscale IC-events. We randomly select 750 event pixels from the observed event and update the pose & motion for  $n_{\text{itr}}$  (1,000) times; it amounts to 0.2% of the dense algorithm. The learning rate  $\eta$  of the  $S, \dot{S}$  is set to  $5 \times 10^{-5}$  exponentially decaying to  $5 \times 10^{-6}$  toward  $n_{\text{itr}}$ . The temporal gradient of intensity w.r.t the event timestamp  $e_u$  is computed by using Pytorch's `autograd.grad`.

```

1 # event: Observed IC-event stream, pose, motion: Initial estimates
2 def TeGRA(event, pose, motion, n_itr=100, eta=5e-4):
3     for itr in range(max_itr):
4         # Compute intensity at event pixel
5         rgb_est = G(event.x, event.y, pose + event.u * motion)
6         # Compute gradient of 'rgb_est' w.r.t event timestamp
7         gradt_est = torch.autograd.grad(rgb_est, event.u)
8         # Compute MSE between estimation and observation
9         loss = mse_loss(gradt_est, event.r)
10        # Compute derivative w.r.t pose and motion
11        loss.backward()
12        # Update pose and motion
13        pose += eta*pose.grad; motion += eta*motion.grad
14    return pose, motion

```

Listing 1. Pseudo-PyTorch Implementation of TeGRA

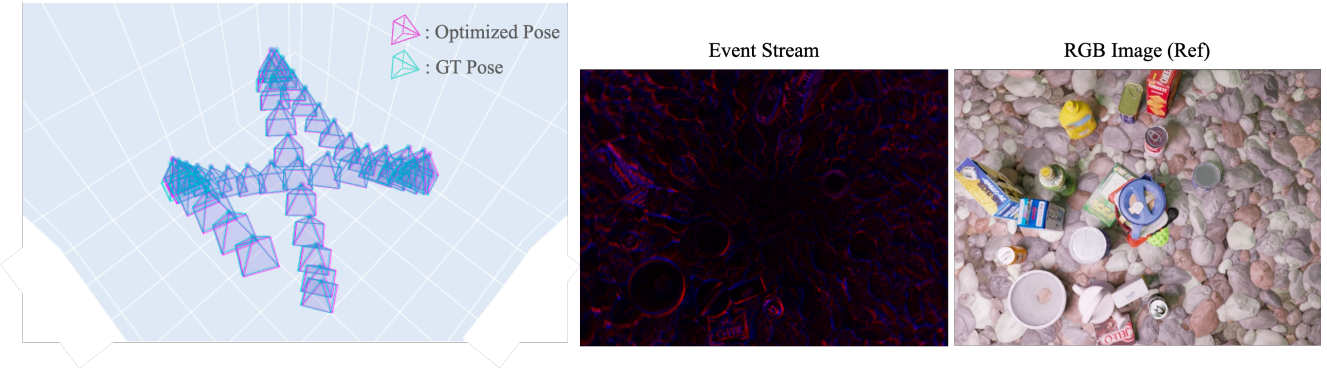


Figure 6. Camera pose tracking results from *mix* scene (Sec.4.3); ground-truth (cyan) and optimized trajectory (magenta) (visualized in every 7 timestep).

### 4.3. Proof of Concept (Tracking)

For the POC of the proposed idea, we applied TeGRA for tracking. We used *seq0* from *mix* scene. We use estimated pose & motion from the previous timestep to initialize ( $S_t^{\text{ini}}, \dot{S}_t^{\text{ini}}$ ) in the next timestep as discussed in Sec.3.3. The results are shown in Fig.6. We confirmed that the pose is successfully tracked without drifting<sup>3</sup>. Finally, the pose estimation error was ( $0.13^\circ, 0.0003$ ). The average number of events per pose update was 0.2% of the entire pixel.

### 4.4. Quantitative Benchmarks (Pose Estimation)

To quantitatively evaluate the performance of the TeGRA, we compare the pose estimation accuracy with the dense algorithm using the difference in intensity (Fig.3). In this experiment, we randomly initialized the pose and motion for each stream. The results are shown in Tab.1. Both achieved comparable accuracy in maintaining camera-pose tracking, while ours used only 2.4% of pixels.

<sup>2</sup>See supplement for network architecture of NeRF (supplement-A.2), and frame-based dense tracking algorithm which we compare the accuracy (supplement-C).

<sup>3</sup>Video for this tracking is included in the supplement. See supplement-F for additional results on NeRF dataset.

## 5. Conclusion

How can we utilize sparse events for recovering the camera pose? Answer: Camera pose is recovered by minimizing the error between the temporal gradient of the scene represented as a NeRF and sparse events. Our tracking algorithm, TeGRA, could update the pose using sparse event points. This mechanism is a significant advantage over the existing image-space algorithm, which requires dense computation. We demonstrate TeGRA in a tracking scenario with unseen background clutter.

We believe the proposed idea opens the door for realizing an event-based camera pose tracking using implicit 3D-scene representation. This study focuses on demonstrating the algorithm in a naive setup; therefore, we left large areas for future work, either from an experimental or algorithmic perspective.

### 5.1. Application to Real-World Data

One of our ultimate goals is to utilize the proposed method in the practical autonomous driving scenario. More specifically, as future work, we plan to apply the TeGRA for Block-NeRF [54], which realized scaling up the NeRF into

Table 1. Pose estimation accuracy comparison of existing dense approach (Fig.3) and our sparse approach (Fig.4, TeGRA).

		<i>hb</i>		<i>lm</i>		<i>tyol</i>		<i>ycbv</i>	
		Rot.	Trans.	Rot.	Trans.	Rot.	Trans.	Rot.	Trans.
Dense	seq0	0.034	0.0002	0.028	0.0004	0.034	0.0003	0.028	0.0003
	seq1	0.036	0.0002	0.562	0.0003	0.033	0.0002	0.567	0.0004
	seq2	0.030	0.0002	0.273	0.0004	0.028	0.0002	0.269	0.0004
Sparse (ours)	seq0	0.217	0.0018	0.321	0.0047	0.350	0.0030	0.760	0.0021
	seq1	0.448	0.0065	0.790	0.0102	0.477	0.0053	0.448	0.0072
	seq2	0.338	0.0054	0.362	0.0088	0.425	0.0058	0.290	0.0051

a city-scale automotive environment. The TeGRA could incorporate the mip-NeRF [6] rendering algorithm, which is key to realizing the large-scale modeling in Block-NeRF. The principle we present (theorem-1) is compatible with a variety of NeRF-variant as long as the 3D-scene is represented in the form of Eq.(2), where  $G_{\mathcal{M}}$  is differentiable w.r.t pose  $S$ .

## 5.2. Asynchronous Update using Binary-Event

In this study, we use IC-event instead of binary-event, and synchronous event stream instead of asynchronous one. We choose this experimental setup mainly due to the implementational difficulties in generating event streams. It requires engineering effort to generate asynchronous binary-event streams, such as modifying event-camera simulators like ESIM [46]. To make the algorithm compatible with the binary polarity  $e_p$ , the loss term in Eq.(5) needs to be modified slightly:

$$\mathcal{L}_{bin} = \sum_i \left\| \text{SoftSgn} \left( \frac{\partial G_{\mathcal{M}} (e_x^i, e_y^i, S_t + \bar{e}_u^i \dot{S}_t)}{\partial \bar{e}_u^i} \right) - e_p^i \right\|_2, \quad (9)$$

where the SoftSgn is a soft version of the sign function, which maps continuous intensity change into (soft) polarity. We left this exploration as future work.

## 5.3. Speed Up

Thanks to the sparse mechanism of TeGRA, the number of pixels to be evaluated for computing the pose update is significantly lower than the entire pixel (Sec.4.3). Speeding up the NeRF for real-time rendering is an active research topic [20, 31, 48, 63]. For example, FastNeRF [20] utilizes a separate network for position-dependent MLP and direction-dependent MLP for speed up. As discussed above, the proposed mechanism is compatible with other NeRF-variants. We expect combining our sparse mechanism with these approaches is a vital topic to realize real-time tracking on mobile devices. We'll incorporate the method and then evaluate the FLOPS and wall-clock time.

## 5.4. Extention to SLAM

It is an exciting research direction to extend our algorithm into simultaneous localization and mapping (SLAM). Now, NeRF is emerging as an entirely new framework for SLAM [30, 52, 57, 66]. iMAP [52] is pioneering work utilizing NeRF for realizing real-time SLAM. We expect incorporating TeGRA will significantly speed up the NeRF-based SLAM.

## References

- [1] I. Alzugaray and M. Chli. Asynchronous multi-hypothesis tracking of features with event cameras. In *Proc. Int. Conf. 3D Vis (DV)*, pages 269–278, 2019. [2](#)
- [2] Ignacio Alzugaray Lopez and Margarita Chli. Haste: multi-hypothesis asynchronous speeded-up tracking of events. In *Proc. Brit. Mach. Vis. Conf. (BMVC)*, page 744, 2020. [2](#)
- [3] Matan Atzmon and Yaron Lipman. Sal: Sign agnostic learning of shapes from raw data. In *Proc. IEEE/CVF Conf. Comput. Vis. Pattern Recognit. (CVPR)*, pages 2565–2574, 2020. [2](#)
- [4] Hendrik Baatz, Jonathan Granskog, Marios Papas, Fabrice Roussel, and Jan Novák. Nerf-tex: Neural reflectance field textures. In *Eurographics Symposium on Rendering (EGSR)*, 2021. [3](#)
- [5] S. Baker and Iain Matthews. Lucas-kanade 20 years on: A unifying framework. *International Journal of Computer Vision (IJCV)*, 56:221–255, 2004. [2](#)
- [6] Jonathan T. Barron, Ben Mildenhall, Matthew Tancik, Peter Hedman, Ricardo Martin-Brualla, and Pratul P. Srinivasan. Mip-nerf: A multiscale representation for anti-aliasing neural radiance fields. In *Proc. IEEE/CVF Int. Conf. Comput. Vis. (ICCV)*, pages 5855–5864, 2021. [7](#)
- [7] Luca Bertinetto, Jack Valmadre, Stuart Golodetz, Ondrej Miksik, and Philip HS Torr. Staple: Complementary learners for real-time tracking. In *Proc. IEEE/CVF Conf. Comput. Vis. Pattern Recognit. (CVPR)*, pages 1401–1409, 2016. [2](#)
- [8] Luca Bertinetto, Jack Valmadre, Joao F Henriques, Andrea Vedaldi, and Philip HS Torr. Fully-convolutional siamese networks for object tracking. In *Proc. Eur. Conf. Comput. Vis. (ECCV)*, pages 850–865, 2016. [2](#)
- [9] Mark Boss, Raphael Braun, Varun Jampani, Jonathan T. Barron, Ce Liu, and Hendrik P.A. Lensch. Nerd: Neural reflectance decomposition from image collections. In *Proc.*

- IEEE/CVF Int. Conf. Comput. Vis. (ICCV)*, pages 12684–12694, 2021. 3
- [10] Samuel Bryner, Guillermo Gallego, Henri Rebecq, and Davide Scaramuzza. Event-based, direct camera tracking from a photometric 3d map using nonlinear optimization. In *Proc. IEEE Int. Conf. Robot. Autom. (ICRA)*, pages 325–331, 2019. 1, 2
- [11] Rohan Chabra, Jan E Lenssen, Eddy Ilg, Tanner Schmidt, Julian Straub, Steven Lovegrove, and Richard Newcombe. Deep local shapes: Learning local sdf priors for detailed 3d reconstruction. In *Proc. Eur. Conf. Comput. Vis. (ECCV)*, pages 608–625, 2020. 2
- [12] William Oswaldo Chamorro Hernandez, Juan Andrade-Cetto, and Joan Solà Ortega. High-speed event camera tracking. In *Proc. Brit. Mach. Vis. Conf. (BMVC)*, pages 1–12, 2020. 2
- [13] Che-Han Chang, Chun-Nan Chou, and Edward Y Chang. Clkn: Cascaded lucas-kanade networks for image alignment. In *Proc. IEEE/CVF Conf. Comput. Vis. Pattern Recognit. (CVPR)*, pages 2213–2221, 2017. 2
- [14] Shoushun Chen and Menghan Guo. Live demonstration: Celex-v: A 1m pixel multi-mode event-based sensor. In *Proc. IEEE/CVF Conf. Comput. Vis. Pattern Recognit. Workshops (CVPRW)*, pages 1682–1683, 2019. 2, 4, 12
- [15] Zhiqin Chen and Hao Zhang. Learning implicit fields for generative shape modeling. In *Proc. IEEE/CVF Conf. Comput. Vis. Pattern Recognit. (CVPR)*, pages 5939–5948, 2019. 2
- [16] Maximilian Denninger, Martin Sundermeyer, Dominik Winkelbauer, Youssef Zidan, Dmitry Olefir, Mohamad Elbadrawy, Ahsan Lodhi, and Harinandan Katam. Blenderproc. 2019. 5, 11
- [17] Terrance DeVries, Miguel Angel Bautista, Nitish Srivastava, Graham W. Taylor, and Joshua M. Susskind. Unconstrained scene generation with locally conditioned radiance fields. *Proc. IEEE/CVF Int. Conf. Comput. Vis. (ICCV)*, 2021. 3
- [18] Guy Gafni, Justus Thies, Michael Zollhofer, and Matthias Nießner. Dynamic neural radiance fields for monocular 4d facial avatar reconstruction. In *Proc. IEEE/CVF Conf. Comput. Vis. Pattern Recognit. (CVPR)*, pages 8649–8658, 2021. 3
- [19] Guillermo Gallego, Jon EA Lund, Elias Mueggler, Henri Rebecq, Tobi Delbrück, and Davide Scaramuzza. Event-based, 6-dof camera tracking from photometric depth maps. *IEEE Trans. Pattern Anal. Mach. Intell.*, 40(10):2402–2412, 2017. 2
- [20] Stephan J Garbin, Marek Kowalski, Matthew Johnson, Jamie Shotton, and Julien Valentin. Fastnerf: High-fidelity neural rendering at 200fps. In *Proc. IEEE/CVF Int. Conf. Comput. Vis. (ICCV)*, pages 14346–14355, 2021. 7
- [21] Daniel Gehrig, Henri Rebecq, Guillermo Gallego, and Davide Scaramuzza. Asynchronous, photometric feature tracking using events and frames. In *Proc. Eur. Conf. Comput. Vis. (ECCV)*, pages 750–765, 2018. 1, 2
- [22] Daniel Gehrig, Henri Rebecq, Guillermo Gallego, and Davide Scaramuzza. Eklt: Asynchronous photometric feature tracking using events and frames. *International Journal of Computer Vision (IJCV)*, 128(3):601–618, 2020. 2
- [23] Tomáš Hodaň, Martin Sundermeyer, Bertram Drost, Yann Labb  , Eric Brachmann, Frank Michel, Carsten Rother, and Ji   Matas. BOP challenge 2020 on 6D object localization. *Proc. Eur. Conf. Comput. Vis. Workshops (ECCVW)*, pages 577–594, 2020. 5, 11
- [24] Jeffrey Ichnowski\*, Yahav Avigal\*, Justin Kerr, and Ken Goldberg. Dex-NeRF: Using a neural radiance field to grasp transparent objects. In *Conference on Robot Learning (CoRL)*, 2020. 3
- [25] Zhang Jiakai, Liu Xinhang, Ye Xinyi, Zhao Fuqiang, Zhang Yanshun, Wu Minye, Zhang Yingliang, Xu Lan, and Yu Jingyi. Editable free-viewpoint video using a layered neural representation. In *SIGGRAPH*, 2021. 3
- [26] Ugur Kart, Alan Lukezic, Matej Kristan, Joni-Kristian Kamarrainen, and Jiri Matas. Object tracking by reconstruction with view-specific discriminative correlation filters. In *Proc. IEEE/CVF Conf. Comput. Vis. Pattern Recognit. (CVPR)*, pages 1339–1348, 2019. 2
- [27] Youngjoong Kwon, Dahun Kim, Duygu Ceylan, and Henry Fuchs. Neural human performer: Learning generalizable radiance fields for human performance rendering. In *Proc. Adv. Neural Inf. Process. Syst. (NeurIPS)*, volume 34, pages 24741–24752, 2021. 3
- [28] Bo Li, Junjie Yan, Wei Wu, Zheng Zhu, and Xiaolin Hu. High performance visual tracking with siamese region proposal network. In *Proc. IEEE/CVF Conf. Comput. Vis. Pattern Recognit. (CVPR)*, pages 8971–8980, 2018. 2
- [29] Zhengqi Li, Simon Niklaus, Noah Snavely, and Oliver Wang. Neural scene flow fields for space-time view synthesis of dynamic scenes. In *Proc. IEEE/CVF Conf. Comput. Vis. Pattern Recognit. (CVPR)*, pages 6498–6508, 2021. 3
- [30] Chen-Hsuan Lin, Wei-Chiu Ma, Antonio Torralba, and Simon Lucey. Barf: Bundle-adjusting neural radiance fields. In *Proc. IEEE/CVF Int. Conf. Comput. Vis. (ICCV)*, pages 5741–5751, 2021. 1, 2, 3, 5, 7
- [31] David B Lindell, Julien NP Martel, and Gordon Wetzstein. Autoint: Automatic integration for fast neural volume rendering. In *Proc. IEEE/CVF Conf. Comput. Vis. Pattern Recognit. (CVPR)*, pages 14556–14565, 2021. 7
- [32] Lingjie Liu, Marc Habermann, Viktor Rudnev, Kripasindhu Sarkar, Jiatao Gu, and Christian Theobalt. Neural actor: Neural free-view synthesis of human actors with pose control. *ACM Trans. Graph. (TOG)*, 40(6):1–16, 2021. 3
- [33] Steven Liu, Xiuming Zhang, Zhoutong Zhang, Richard Zhang, Jun-Yan Zhu, and Bryan Russell. Editing conditional radiance fields. In *Proc. IEEE/CVF Int. Conf. Comput. Vis. (ICCV)*, pages 5773–5783, 2021. 3
- [34] Bruce D. Lucas and Takeo Kanade. An iterative image registration technique with an application to stereo vision. In *Proc. Int. Joint Conf. Artif. Intell. (IJCAI)*, volume 2, page 674–679, 1981. 2
- [35] Lars Mescheder, Michael Oechsle, Michael Niemeyer, Sebastian Nowozin, and Andreas Geiger. Occupancy networks: Learning 3d reconstruction in function space. In *Proc. IEEE/CVF Conf. Comput. Vis. Pattern Recognit. (CVPR)*, pages 4460–4470, 2019. 2
- [36] Ben Mildenhall, Pratul P. Srinivasan, Rodrigo Ortiz-Cayon, Nima Khademi Kalantari, Ravi Ramamoorthi, Ren Ng, and

- Abhishek Kar. Local light field fusion: Practical view synthesis with prescriptive sampling guidelines. *ACM Trans. Graph. (TOG)*, 2019. 2
- [37] Ben Mildenhall, Pratul P Srinivasan, Matthew Tancik, Jonathan T Barron, Ravi Ramamoorthi, and Ren Ng. Nerf: Representing scenes as neural radiance fields for view synthesis. In *Proc. Eur. Conf. Comput. Vis. (ECCV)*, pages 405–421, 2020. 1, 2, 4, 11, 13
- [38] Michael Niemeyer and Andreas Geiger. Giraffe: Representing scenes as compositional generative neural feature fields. In *Proc. IEEE/CVF Conf. Comput. Vis. Pattern Recognit. (CVPR)*, pages 11453–11464, 2021. 2
- [39] Michael Oechsle, Songyou Peng, and Andreas Geiger. Unisurf: Unifying neural implicit surfaces and radiance fields for multi-view reconstruction. In *Proc. IEEE/CVF Int. Conf. Comput. Vis. (ICCV)*, pages 5589–5599, 2021. 3
- [40] Jeong Joon Park, Peter Florence, Julian Straub, Richard Newcombe, and Steven Lovegrove. Deepsdf: Learning continuous signed distance functions for shape representation. In *Proc. IEEE/CVF Conf. Comput. Vis. Pattern Recognit. (CVPR)*, pages 165–174, 2019. 2
- [41] Keunhong Park, Utkarsh Sinha, Jonathan T. Barron, Sofien Bouaziz, Dan B Goldman, Steven M. Seitz, and Ricardo Martin-Brualla. Nerfies: Deformable neural radiance fields. In *Proc. IEEE/CVF Int. Conf. Comput. Vis. (ICCV)*, pages 5865–5874, 2021. 3
- [42] Adam Paszke, Sam Gross, Francisco Massa, Adam Lerer, James Bradbury, Gregory Chanan, Trevor Killeen, Zeming Lin, Natalia Gimelshein, Luca Antiga, Alban Desmaison, Andreas Kopf, Edward Yang, Zachary DeVito, Martin Raison, Alykhan Tejani, Sasank Chilamkurthy, Benoit Steiner, Lu Fang, Junjie Bai, and Soumith Chintala. Pytorch: An imperative style, high-performance deep learning library. In H. Wallach, H. Larochelle, A. Beygelzimer, F. d’Alché-Buc, E. Fox, and R. Garnett, editors, *Proc. Adv. Neural Inf. Process. Syst. (NeurIPS)*, pages 8024–8035, 2019. 5
- [43] Christoph Posch, Daniel Matolin, and Rainer Wohlgenannt. High-dr frame-free pwm imaging with asynchronous aer intensity encoding and focal-plane temporal redundancy suppression. In *International Symposium on Circuits and Systems (ISCAS)*, pages 2430–2433, 2010. 2
- [44] Prophesee metavision for machines. <https://www.prophesee.ai/>. 2
- [45] Albert Pumarola, Enric Corona, Gerard Pons-Moll, and Francesc Moreno-Noguer. D-nerf: Neural radiance fields for dynamic scenes. In *Proc. IEEE/CVF Conf. Comput. Vis. Pattern Recognit. (CVPR)*, pages 10318–10327, 2021. 3
- [46] Henri Rebecq, Daniel Gehrig, and Davide Scaramuzza. Esim: An open event camera simulator. In *Conference on Robot Learning (CoRL)*, pages 969–982, 2018. 7
- [47] Henri Rebecq, Timo Horstschaefer, and Davide Scaramuzza. Real-time visual-inertial odometry for event cameras using keyframe-based nonlinear optimization. In *Proc. Brit. Mach. Vis. Conf. (BMVC)*, 2017. 2
- [48] Sara Fridovich-Keil and Alex Yu, Matthew Tancik, Qinhong Chen, Benjamin Recht, and Angjoo Kanazawa. Plenoxels: Radiance fields without neural networks. In *Proc. IEEE/CVF Conf. Comput. Vis. Pattern Recognit. (CVPR)*, 2022. 7
- [49] Teresa Serrano-Gotarredona and Bernabé Linares-Barranco. A  $128 \times 128$  1.5% contrast sensitivity 0.9% fpn 3  $\mu$ s latency 4 mw asynchronous frame-free dynamic vision sensor using transimpedance preamplifiers. *IEEE Journal of Solid-State Circuits (JSSC)*, 48(3):827–838, 2013. 2
- [50] Vincent Sitzmann, Julien Martel, Alexander Bergman, David Lindell, and Gordon Wetzstein. Implicit neural representations with periodic activation functions. In *Proc. Adv. Neural Inf. Process. Syst. (NeurIPS)*, volume 33, pages 7462–7473, 2020. 2
- [51] Pratul P Srinivasan, Boyang Deng, Xiuming Zhang, Matthew Tancik, Ben Mildenhall, and Jonathan T Barron. Nerv: Neural reflectance and visibility fields for relighting and view synthesis. In *Proc. IEEE/CVF Conf. Comput. Vis. Pattern Recognit. (CVPR)*, pages 7495–7504, 2021. 3
- [52] Edgar Sucar, Shikun Liu, Joseph Ortiz, and Andrew J Davison. imap: Implicit mapping and positioning in real-time. In *Proc. IEEE/CVF Int. Conf. Comput. Vis. (ICCV)*, pages 6229–6238, 2021. 3, 7
- [53] Yunjae Suh, Seungnam Choi, Masamichi Ito, Jeongseok Kim, Youngho Lee, Jongseok Seo, Heejae Jung, Dong-Hee Yeo, Seol Namgung, Jongwoo Bong, et al. A  $1280 \times 960$  dynamic vision sensor with a  $4.95\text{-}\mu\text{m}$  pixel pitch and motion artifact minimization. In *International Symposium on Circuits and Systems (ISCAS)*, 2020. 2
- [54] Matthew Tancik, Vincent Casser, Xinchen Yan, Sabeek Pradhan, Ben Mildenhall, Pratul Srinivasan, Jonathan T. Barron, and Henrik Kretzschmar. Block-NeRF: Scalable large scene neural view synthesis. 2022. 1, 3, 6
- [55] Paul Voigtlaender, Jonathon Luiten, Philip HS Torr, and Bastian Leibe. Siam r-cnn: Visual tracking by re-detection. In *Proc. IEEE/CVF Conf. Comput. Vis. Pattern Recognit. (CVPR)*, pages 6578–6588, 2020. 2
- [56] Peng Wang, Lingjie Liu, Yuan Liu, Christian Theobalt, Taku Komura, and Wenping Wang. Neus: Learning neural implicit surfaces by volume rendering for multi-view reconstruction. In *Proc. Adv. Neural Inf. Process. Syst. (NeurIPS)*, 2021. 3
- [57] Zirui Wang, Shangzhe Wu, Weidi Xie, Min Chen, and Victor Adrian Prisacariu. Nerf-: Neural radiance fields without known camera parameters. 2021. 3, 7
- [58] Yi Wei, Shaohui Liu, Yongming Rao, Wang Zhao, Jiwen Lu, and Jie Zhou. Nerfingmvs: Guided optimization of neural radiance fields for indoor multi-view stereo. In *Proc. IEEE/CVF Int. Conf. Comput. Vis. (ICCV)*, pages 5610–5619, 2021. 3
- [59] Suttisak Wizadwongsu, Pakkapon Phongthawee, Jiraphon Yenpraphai, and Supasorn Suwajanakorn. Nex: Real-time view synthesis with neural basis expansion. In *Proc. IEEE/CVF Conf. Comput. Vis. Pattern Recognit. (CVPR)*, pages 8534–8543, 2021. 3
- [60] Christopher Xie, Keunhong Park, Ricardo Martin-Brualla, and Matthew Brown. Fig-nerf: Figure-ground neural radiance fields for 3d object category modelling. In *International Conference on 3D Vision (3DV)*, pages 962–971, 2021. 3
- [61] Bangbang Yang, Yinda Zhang, Yinghao Xu, Yijin Li, Han Zhou, Hujun Bao, Guofeng Zhang, and Zhaopeng Cui. Learning object-compositional neural radiance field for ed-

- itable scene rendering. In *Proc. IEEE/CVF Int. Conf. Comput. Vis. (ICCV)*, pages 13779–13788, 2021. 3
- [62] Lin Yen-Chen, Pete Florence, Jonathan T. Barron, Alberto Rodriguez, Phillip Isola, and Tsung-Yi Lin. iNeRF: Inverting neural radiance fields for pose estimation. In *Proc. IEEE/RSJ Int. Conf. Intell. Robots Syst. (IROS)*, pages 1323–1330, 2021. 1, 2, 3
- [63] Alex Yu, Rui long Li, Matthew Tancik, Hao Li, Ren Ng, and Angjoo Kanazawa. PlenOctrees for real-time rendering of neural radiance fields. In *Proc. IEEE/CVF Int. Conf. Comput. Vis. (ICCV)*, pages 5752–5761, 2021. 7
- [64] Xiuming Zhang, Pratul P Srinivasan, Boyang Deng, Paul Debevec, William T Freeman, and Jonathan T Barron. Nerfactor: Neural factorization of shape and reflectance under an unknown illumination. *ACM Trans. Graph. (TOG)*, 40(6):1–18, 2021. 3
- [65] Shuaifeng Zhi, Tristan Laidlow, Stefan Leutenegger, and Andrew Davison. In-place scene labelling and understanding with implicit scene representation. In *Proc. IEEE/CVF Int. Conf. Comput. Vis. (ICCV)*, pages 15838–15847, 2021. 3
- [66] Zihan Zhu, Songyou Peng, Viktor Larsson, Weiwei Xu, Hujun Bao, Zhaopeng Cui, Martin R Oswald, and Marc Pollefeys. Nice-slam: Neural implicit scalable encoding for slam. In *Proc. IEEE/CVF Conf. Comput. Vis. Pattern Recognit. (CVPR)*, pages 12786–12796, 2022. 3, 7
- [67] Alex Zihao Zhu, Nikolay Atanasov, and Kostas Daniilidis. Event-based visual inertial odometry. In *Proc. IEEE/CVF Conf. Comput. Vis. Pattern Recognit. (CVPR)*, pages 5391–5399, 2017. 2

## A. NeRF

### A.1. NeRF Formulation

NeRF [37] is an implicit 3D scene representation using neural networks, originally proposed for novel view synthesis. As in Sec.3.1, NeRF,  $G_M$ , takes an image coordinate  $(x, y)$  and 6DoF pose  $S \in \mathfrak{se}(3)$  of the camera as inputs and render the RGB intensity  $\mathbf{c}$  at that coordinate. NeRF encodes a 3D scene as a continuous representation using an MLP  $f_M$ , parameterized by learned parameter  $M$ . The  $f_M$  output the intensity  $\mathbf{c}'$  and volume density  $\sigma$  given a viewing ray  $\mathbf{d}$  and a 3D coordinate  $\mathbf{x}$ . The viewing ray  $\mathbf{d}$  is computed from the camera pose  $S$  and image coordinate  $(x, y)$ . Let the homogeneous image coordinate  $\bar{\mathbf{u}} = (x, y, 1)$ ; then, the 3D point  $\mathbf{x}^i$  along the viewing ray  $\mathbf{d}$  at depth  $z^i$  is expressed as  $\mathbf{x}^i = \bar{\mathbf{u}} + z^i \mathbf{d}$ . NeRF integrate the intensity  $\mathbf{c}'$  using density  $\sigma$  by volume rendering to obtain intensity at the image coordinate  $(x, y)$  for the given camera pose  $S$  as follows:

$$G_M(x, y, S) = \int_{z_n}^{z_f} T(z) \sigma(\bar{\mathbf{u}} + z \mathbf{d}) \mathbf{c}'(\bar{\mathbf{u}} + z \mathbf{d}) dz, \quad (1)$$

$$T(z) = \exp \left( - \int_{z_n}^z \sigma(\bar{\mathbf{u}} + z' \mathbf{d}) dz' \right) \quad (2)$$

where,  $z_n$  and  $z_f$  are bounds on the depth range of interest. In practice, this rendering function is approximated numerically via quadrature on points in the depth direction.

### A.2. Network Architecture

The NeRF network architecture used for the experiments is shown in Fig.A. We adopt code of NeRF from BARF official implementation <https://github.com/chenhsuanlin/bundle-adjusting-NeRF> for training the model. The difference from the original NeRF [37] is activation for density  $\sigma$  is replaced by softplus from relu to improve stability during training. The function  $\gamma$  is a positional encoding function that maps inputs 3D coordinates  $x$  to higher dimensions of different sinusoidal frequency basis functions.

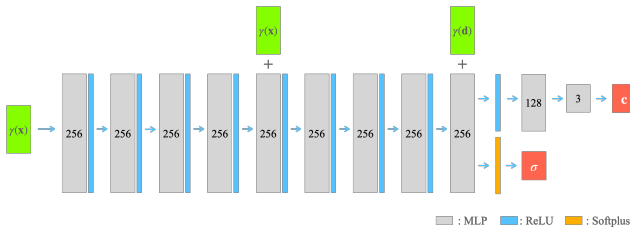


Figure A. The NeRF network architecture used for the experiments.

## B. Event-based camera pose tracking dataset (EvTrack)

We created the 6DOF camera pose tracking dataset for event data, called EvTrack, with ground-truth camera pose to demonstrate the effectiveness of the proposed TeGRA and foster subsequent studies of event-based camera pose tracking using implicit 3D scene representation.

We used BOP challenge 2020 scenes [23] because it is photo-realistic, and the scene represents the indoor localization scenario well. The BOP 2020 uses the Blender-Proc [16] to render realistic images using ray-tracing. The dataset consists of five scenes, *mix*, *hb*, *lm*, *tyol* and *ycbb*, the last four scenes correspond to the BOP data split and *mix* scenes include all the four data to simulate the ordinary indoor situation.

### B.1. Data for training

The training data consists of 500 images with ground-truth camera poses for each scene. Each camera pose is randomly sampled from a pre-defined rectangular space that includes the tracking trajectories described in B.2. The size of image ( $H, W$ ) is  $(480 \times 640)$ . An implicit 3D scene representation such as NeRF can be trained using the data.

### B.2. Data for testing (tracking)

The test data consists of three camera trajectories for each scene simulating the drone hovering around a room (Fig.6 right). For each scene, we render 1,000 consecutive images with ground-truth camera poses. The size of image ( $H, W$ ) is  $(480 \times 640)$ . Using the consecutive images, we generate IC-event by subtracting the successive frames. The threshold  $\delta$  for triggering the event is set to 0.05 (intensities are normalized to  $[0, 1]$ ) for all scenes.

In our experiment, we use grayscale IC-event since most event cameras detect grayscale intensity changes. To generate a grayscale IC-event, we convert the RGB frame into a grayscale frame using OpenCV's `cvtColor()` function.

### B.3. Chunk size

The number of events consumed by the network at once (chunk size) must be determined depending on the scene. In general, we can expect a higher accuracy when using a longer chunk size as long as the chunked event stream conforms to the motion model (we used the linear model of (5) in our experiment). On the other hand, when the chunk size is too large, and the chunked event stream contains non-linear motion, the observed event can not be explained by the motion model, and the performance will degrade. We use *four* timestep (generated from five consecutive frames) in our main experiment. The camera motion in the EvTrack can be considered approximately linear within the *five* frame interval.

#### B.4. Required accuracy for tracking

In the main paper, we discussed both dense approach and our sparse approach to achieve comparable accuracy to keep the tracking (although their pose error differs). The pose error from TeGRA is larger than the dense approach because the observed event trajectory does not precisely conform to the motion model we use (linear motion model), while the dense model aligns a single image without temporal information (therefore, there is no model error). One could utilize a non-linear motion model to reduce the error further. However, the error from TeGRA is sufficiently small to keep stable tracking; therefore, the linear model suffices for tracking (on the EvTrack dataset). Tab.B show the tracking results on all the sequences in the EvTrack. We consider the pose is successfully tracked ( $\checkmark$ ) if the error in the final pose is less than the initial pose error of  $(1.0^\circ, 0.001)$  (Due to the time required to run the dense RGB method (Fig.3), we used the randomly sampled 50 consecutive frames from each sequence).

We also confirmed that TeGRA could successfully track the camera pose without drifting on the NeRF’s blender scene (supplement-F).

Table B. Tracking test of dense approach (Fig.3) and our sparse approach (Fig.4, TeGRA).

	<i>mix</i>	<i>hb</i>	<i>lm</i>	<i>tyol</i>	<i>ycbv</i>
Dense	seq0	$\checkmark$	$\checkmark$	$\checkmark$	$\checkmark$
	seq1	$\checkmark$	$\checkmark$	$\checkmark$	$\checkmark$
	seq2	$\checkmark$	$\checkmark$	$\checkmark$	$\checkmark$
Sparse (ours)	seq0	$\checkmark$	$\checkmark$	$\checkmark$	$\checkmark$
	seq1	$\checkmark$	$\checkmark$	$\checkmark$	$\checkmark$
	seq2	$\checkmark$	$\checkmark$	$\checkmark$	$\checkmark$

#### C. Tracking using dense image

As discussed in the Sec.1 and (Fig.3), camera pose can be recovered using NeRF and dense intensity observation. We use the same pre-trained NeRF model as our TeGRA and estimate the camera pose  $S$ . Unlike ours, which optimizes pose  $S$  and motion  $\dot{S}$ , the frame-based algorithm only optimizes pose  $S$ . Because the entire  $480 \times 640$  pixels can not fit into the single GPU, we split the pixels into a 4,000-pixel chunk and accumulated the gradient w.r.t.  $S$  to compute the single pose update for a frame. The pose update is repeated  $n\_itr$  (100) times for each observed frame. The learning rate  $\eta$  of the  $S$  is set to  $5 \times 10^{-4}$  exponentially decaying to  $5 \times 10^{-5}$  toward  $n\_itr$ .

#### D. Binary Event to IC-Event

In this study, we use IC-event instead of binary-event, and synchronous event stream instead of asynchronous one. We choose this experimental setup mainly due to the implementational difficulties in generating event streams. It requires engineering effort to generate asynchronous binary-event streams, such as modifying event-camera simulators. Some event-based cameras can detect the intensity change  $e_r$  directly, such as Celex-V [14]. However, perhaps the most common type reports an event  $e = [e_x, e_y, e_t, e_p]^\top$  when it detects the intensity change  $\Delta L$  by a specified amount  $\delta$ , where  $e_p \in [+1, -1]$  is the polarity which indicates the increase or decrease of the intensity changes.

We consider there are two possible approaches to make TeGRA compatible with the binary-event; 1) Modify the loss function of (5) to adapt to the binary-event (Sec.5.2), 2) Convert the binary-event to IC-event using the timestamp (supplement-D). In this work, we use IC-event for simplicity and left the exploration for future work.

In this section, we discuss the second approach. IC-event could be estimated by a simple (linear fitting). One can use the time difference between the latest two consecutive events on each pixel to estimate the intensity difference, as depicted in Fig.D. There are other options, such as fitting higher-order functions using more events.

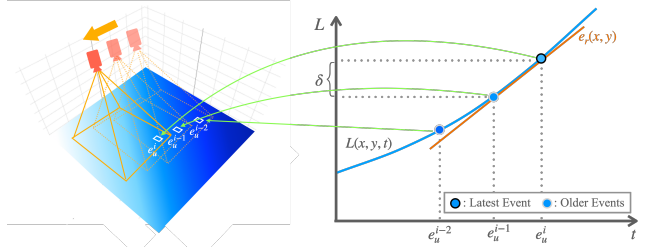


Figure D. Binary-Event to IC-Event

## E. Algorithm of TeGRA

The complete algorithm of TeGRA is listed in Alg.E. Note that the algorithm listed in Alg.E is slightly different from the one we used in our main experiment (listing-1). In the main experiments, we used a fixed number of iterations for a fair comparison; however, we expect terminating iteration using the norm of the pose & motion update is preferable for the practical application in terms of computational efficiency.

---

### Algorithm E TeGRA

---

**Input:** IC-event stream  $\mathbf{e}_t$

Optimized pose & motion  $(S_{t-\nu}^{\text{opt}}, \dot{S}_{t-\nu}^{\text{opt}})$  at time  $t - \nu$

- 1:  $\epsilon \leftarrow \inf$
- 2:  $(S_t^{\text{ini}}, \dot{S}_t^{\text{ini}}) \leftarrow (S_{t-\nu}^{\text{opt}} + \nu \dot{S}_{t-\nu}^{\text{opt}}, \dot{S}_{t-\nu}^{\text{opt}})$   $\triangleright$ (linear motion)
- 3:  $(S, \dot{S}) \leftarrow (S_t^{\text{ini}}, \dot{S}_t^{\text{ini}})$
- 4: **while**  $\epsilon > \epsilon_{thr}$  **do**
- 5:   Feedward event coordinate and pose to  $G_{\mathcal{M}}$
- 6:   Compute temporal gradient of  $G_{\mathcal{M}}$  w.r.t  $[..., \bar{e}_u^i, ...]$
- 7:   Evaluate error between  $\nabla_t \text{NeRF}(S_t)$  and IC-event  $\triangleright$ Eq.(5)
- 8:   Backpropagete the error through  $\nabla_t \text{NeRF}(S_t)$
- 9:   Update pose & motion
- 10:    $\epsilon \leftarrow$  norm of pose & motion update
- 11: **end while**
- 12:  $(S_t^{\text{opt}}, \dot{S}_t^{\text{opt}}) \leftarrow (S, \dot{S})$

**Output:**  $(S_t^{\text{opt}}, \dot{S}_t^{\text{opt}})$

---

## F. Additional tracking result on NeRF dataset

In addition to the main tracking experiment using Event-Track, we also conducted an experiment to evaluate the tracking performance of TeGRA on the NeRF’s blender scene [37]. For this experiment, we created the event stream from 1,000 consecutive frames using the blender scene; the camera rotates around the object while moving up and down. We also confirmed that the camera pose is successfully tracked without drift on this dataset (Fig.F, See also supplemental video).

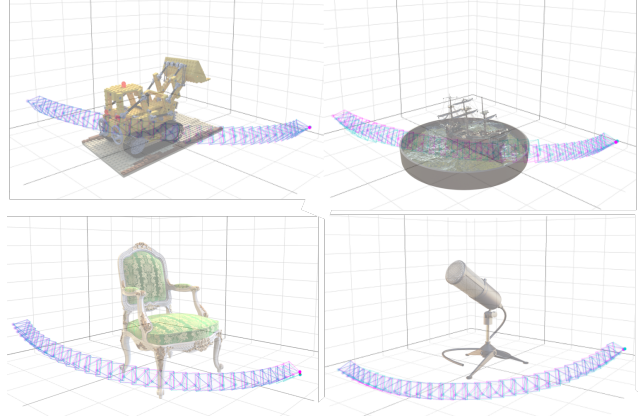


Figure F. Additional tracking results on NeRF’s blender scene.